Ge Nanodots Embedded in a Silica Matrix

I. STAVARACHE, A.-M. LEPADATU, M.L. CIUREA

National Institute of Materials Physics, 105 bis Atomistilor Street,
Magurele 077125, Romania

Tel: +40-21-3690185; Fax: +40-21-3690177
E-mail: ciurea@infim.ro

Abstract. The properties of GeSiO films consisting of Ge nanodots embedded in SiO_2 matrix, prepared by sol-gel and magnetron sputtering methods, followed by an adequate thermal annealing, are studied and discussed in this paper. Structural investigations were performed by means of transmission electron microscopy and X-ray photoelectron spectroscopy. In the sol-gel films one finds amorphous Ge nanodots distributed in the amorphous matrix, while in the sputtered ones tetragonal Ge nanodots are evidenced. The electrical and photoconductive properties of sol-gel films treated by rapid thermal annealing technique were also studied. For this, measurements of current-voltage and conductance-temperature curves, spectral and bias dependences of the photocurrent were carried out. These films have weak rectifying behaviour and show a very high photoconductivity.

Keywords: Nanodots; Sol-gel; Magnetron sputtering; TEM; XPS; Photoconductive nanostructures; Electrical properties; Photoelectrical properties.

1. Introduction

Much research in recent years has focused on films consisting of Ge nanodots embedded in SiO_2 matrix. Many studies on synthesis methods [1−2], structural aspects [3−6] and optical properties [3−4, 7−8] of these structures were reported. The memory effect related to charge storage [6−7, 9−10], electrical [9−13] and photoconductive [14−15] properties were also investigated. These films can be prepared using different methods: sol-gel [1, 3, 5−6, 16], molecular beam epitaxy [9−10, 14, 17−18], magnetron sputtering [2, 4, 5, 7−8, 12, 19], plasma-enhanced chemical vapor deposition [20], atom beam co-sputtering [21], and Ge implantation [22] and/or combined with neutron irradiation [23]. Different annealing techniques are used for Ge nanodots formation such as furnace annealing [6], rapid thermal annealing (RTA) [6, 16], or microwave annealing [24]. Ge nanodots can be also

embedded in other oxide matrixes, *e.g.* HfO_2 [25−26], Al_2O_3 [27] or TiO_2 [28]. The films of Ge nanocrystals embedded in SiO_2 present a wide range of possible applications, in MOS based gamma radiation sensors [29], heterojunction devices with photovoltaic effects for solar cells [13], MOS-structure photodiodes for optoelectronics [30], and nonvolatile memories [6, 31].

The magnetron sputtering films containing Ge nanodots embedded in silicon dioxide are obtained in a wide range of different deposition and annealing conditions. The deposition conditions depend on the type of the used target and on the ambient atmosphere. One can use a target of SiO_2 covered with Ge pieces [5, 12−13, 19], two targets of SiO_2 and Ge respectively [4, 8], a Si target covered with Ge chips using a reactive co-sputtering [7]. Argon is commonly used as a sputtering gas [8, 12] or a mixture of different gases (Ar, O_2) is used in a reactive sputtering [7]. Other deposition parameters are also important for the structure, microstructure and properties of the films (the RF power, the substrate temperature [7, 13].

Cosentino et al [8] synthesized Ge quantum dots (2–10 nm) embedded in silica by magnetron co-sputtering of SiO_2 and Ge, in Ar atmosphere, followed by annealing at 600–800°C in N_2. Zhang et al [13] obtained thin films composed of quasi-spherical Ge nanocrystals (3.8–8 nm), with diamond structure, distributed in SiO_2, by magnetron co-sputtering from a fused quartz plate partially covered with Ge chips (undoped or doped with Ga or Sb). During the deposition, the substrates were heated at 380°C and, then, the obtained films were annealed by RTA method in N_2 at 650–800°C. Ray et al [7] prepared nearly spherical Ge nanocrystals (4–7 nm) embedded in SiO_2 matrix by reactive RF magnetron co-sputtering from a n-type Si wafer target covered with Ge pieces, using a mixture of oxygen and argon. Then, the deposited films were annealed in N_2 for 1h at 600–900°C. Kolobov et al [4] prepared films of Ge nanocrystals (5–20 nm) embedded in SiO_2 also by co-sputtering of Ge and SiO_2, with a subsequent annealing at 800°C in Ar. The films contain 25, 40 or 60 mol% of Ge in the SiO_2 matrix. The authors found that the size of nanocrystals strongly depends on the type of the used substrate, Si (100). Ge nanocrystals with two shapes were observed, ones are spherical with multiple twinning defects and the other ones are faceted single crystals. They have also evidenced a gradient of Ge nanocrystals concentration with the depth of the film. At the film's surface, there are no Ge nanocrystals, and at the bottom part, i.e. at the interface with the Si substrate, a higher density of Ge nanocrystals was evidenced. The authors observed the presence of single faceted nanocrystals in the layer, whereas at the interface with the Si substrate, spherical nanocrystals with multiple twinning defects are present. The films deposited on quartz substrates have Ge nanocrystals with smaller sizes that form a continuous network. Shen et al [19] obtained Ge nanocrystals (2.1–27.2 nm) with diamond structure by co-sputtering of SiO_2 and Ge, followed by an annealing in N_2 at different temperatures (300–1100°C). They remarked the out-diffusion of Ge atoms in the samples

annealed at 1100°C. The same system was prepared by Fujii *et al* [12] using a thermal annealing at 800°C in vacuum, resulting Ge nanocrystals with sizes of 3.8–8.9 nm.

Cosentino et al studied the influence of surfaces states on the photon absorption in films formed of Ge nanoclusters embedded in silica [8]. The authors found an optical bandgap of 1.6 eV, independent on the quantum dot size (for size in 2−10 nm range) and the structural phase, amorphous or crystalline (diamond) of Ge nanoclusters. They showed how the absorption is influenced by surface states. The authors also observed the Ge out-diffusion through the surface.

Zhang et al studied the electrical properties of undoped and doped thin films of Ge nanocrystals embedded in SiO$_2$ [13]. The undoped films treated by RTA exhibit a p-type conductivity (σ), with about three orders of magnitude higher than those as-deposited. They measured current – voltage (*I–V*) characteristics of films treated in 650–800°C range. The *I–V* curves are linear except the one with RTA at 800°C which presents a small non-linearity at low voltages. This behaviour was attributed to the acceptor-like surface states which produce the holes accumulation in nanocrystals. They evidenced a thermally activated process, given by the $\ln \sigma \sim T^{-1}$ law, explained by a hopping process from one nanocrystal to its nearest neighbour one. In the (Ga or Sb) doped layers, similar electrical behaviour was found, explained by the major influence of surface states which determine a dominant hole conduction, too. They evidenced a clear photovoltaic effect given by the heterojunction between p-type SiO$_2$ films with Ge nanocrystals and n-type silicon wafer.

Ray *et al* investigated a trilayer MOS capacitor [7] that consists of a tunnel oxide thermally grown on a p-Si substrate, an intermediate layer composed of Ge nanocrystals with 20–30 nm diameters, and a cap gate oxide. These structures annealed by RTA exhibit a strong and broad photoluminescence (PL) at room temperature (RT), attributed to quantum confinement of carriers in Ge nanocrystals. If the annealing time is increased, the films present a narrower PL spectrum.

Electroluminescence (EL) was investigated by Shen et al [19] in a metal-insulator-semiconductor (MIS) structure. The films treated by RTA at different temperatures in the range of 300–1100°C present a broad maximum centred at 590 nm. For the films annealed at 600°C, the EL intensity (590 nm) is much higher. Also, the EL intensity rapidly decreases with the nanocrystal size increase. The authors explained the EL curves by a radiative recombination in the small Ge nanocrystals.

Fujii *et al* [11−12] find variable range hopping (VRH) conduction mechanism, $\ln \sigma \propto T^{-1/4}$, through localized states associated with Ge clusters, in the as-deposited films of Ge clusters embedded in SiO$_2$. In the annealed films, containing Ge nanocrystals, the $\ln \sigma \propto T^{-1/2}$ dependence was evidenced [12].

They explained the electrical conduction as due to the tunneling of carriers between neighboring nanocrystals.

Other method to prepare films formed of Ge nanodots embedded in SiO_2 matrix is the sol-gel method [1, 3, 5−6, 15−16]. Different precursors for Ge and Si were used, germanium tetraethoxide $Ge(OC_2H_5)_4$ [6], 3-trichlorogermanium propanoic acid $Cl_3−Ge−C_2H_4−COOH$ [3] or $GeCl_4$ 1, 5, 15] and/or silicon tetraethoxide TEOS $Si(OC_2H_5)_4$ [1, 3, 5−6, 15−16] or dimethyldiethoxysilane $(CH_3)_2Si(OC_2H_5)_2$ [6] respectively. The values of the Ge/Si molar ratio in solution are relatively small, in the interval of 3 – 15 % [1, 3, 5, 15−16]. The SiO_2-GeO_2 gel films are deposited either by means of dip coating method [6] or spin coating [5, 15−16] on different substrates, commonly used being Si (100) wafers [5−6, 16]. After the deposition, the films are annealed under different conditions of temperature and gas atmosphere: 400 – 800°C, in a flowing mixed gas of H_2 and N_2 [1, 3, 5−6] or 800°C and 950°C in Ar and N_2 atmosphere [15−16].

Investigations of structure and microstructure and optical studies were performed on the sol-gel films consisting of Ge nanodots embedded in SiO_2. The crystallinity of Ge nanodots was evidenced by high resolution transmission electron microscopy (HRTEM) and selected area electron diffraction (SAED). Thus, Ge nanodots with diamond structure [1, 3], amorphous Ge nanodots distributed in the SiO_2 amorphous matrix [16] and Ge nanodots with tetragonal phase [5, 15] were reported in literature. Knebel et al [6] observed two shapes of Ge nanocrystals, ones being globular and the others strongly faceted with tetrahedral form. However, films with small spherical Ge nanodots (up to 10 nm) dispersed in the amorphous matrix are usually obtained [1, 5, 15−16].

These films exhibit PL: Nogami *et al* reported visible PL [1] at liquid nitrogen temperature and Yang *et al* [3] observed a strong visible PL at RT. Surprisingly, the films with Ge nanocrystals having a diamond structure are not photoluminescent.

In this paper, we present the properties of GeSiO films consisting of Ge nanodots embedded in amorphous SiO_2 matrix, prepared by sol-gel and magnetron sputtering methods. Structural investigations were performed by means of transmission electron microscopy (TEM) and X-ray photoelectron spectroscopy (XPS) methods. In the sol-gel films we obtained amorphous Ge nanodots distributed in the amorphous matrix, while in the sputtered ones appeared both tetragonal Ge nanodots and a network of Ge-rich amorphous nanostructures. The electrical and photoconductive properties of sol-gel GeSiO films treated by RTA technique were also studied. To do that, measurements of $I – V$ and conductance-temperature ($G – T$) curves, spectral ($I_f – \lambda$) and bias dependences ($I_f – V$) of the photocurrent were carried out. These films have weak rectifying behaviour and show a very high photoconductivity.

2. Experimental: Preparation and Measurements

In order to prepare GeSiO thin films, two conventional methods, *i.e.* the sol–gel [15−16, 32] and the radio frequency magnetron sputtering methods [5, 32] were used. The film deposition was followed by an annealing process in order to allow Ge segregation as well as Ge nanodots formation.

The sol-gel method for the preparation of GeSiO layers, $GeCl_4$ and tetraethyl orthosilicate $Si(OC_2H_5)_4$ (TEOS) as precursors, dissolved in ethanol were used. The two sols of GeO_2 and SiO_2 were mixed, for different values of the Ge/Si molar ratio, in the $3 - 12$ % interval, depending on the desired Ge content in the film. The final mixture was stirred at RT, and then, it was deposited on silicon substrates by using the spin coating method. After this stage, the films were dried and heated in air at $400 - 600^{o}C$ in order to remove the organic solvent. The resulting GeO_2-SiO_2 films were compact and homogeneous. Then, some films were annealed in N_2 atmosphere at $800 - 950^{o}C$, using a RTA for $5 - 15$ min. An alternative annealing was made in N_2 at $1000^{o}C$ for 7 h in a heater, or in H_2 (at 2 atm and $500^{o}C$). The thickness of the GeSiO layers ranged between 200 and 300 nm. Al electrodes were deposited in a planar geometry on RTA annealed samples, for electrical and photoconductivity measurements.

The sputtered GeSiO films were prepared by using a target consisting of a SiO_2 disk with germanium pieces fixed on it. The Ge area covering the sputtering active zone was chosen in order to obtain a desired mass concentration of Ge/SiO_2 of 40 %. The deposition was performed in high purity argon atmosphere (99.99 %). An argon pressure of 0.3 Pa was maintained during the deposition. A constant power of 150 W RF was used at a generator frequency of 1.78 MHz. These films were deposited on silica substrates, placed at 35 mm above the target. Again, similarly with the sol-gel case, the films were annealed in a H_2 atmosphere (at 2 atm and $500^{o}C$). The sputtered GeSiO films are much thicker (about 3 μm) than the sol-gel ones.

The microstructure of the GeSiO layers with different Ge concentrations was investigated by means of TEM and HRTEM. Two different methods were used for the preparation of the TEM sol-gel specimens: some of them were prepared by a cross section method, and those used for plan view investigations by ion milling using a Gatan PIPS 691 apparatus. In the case of magnetron sputtered GeSiO layers, being much thicker, the TEM specimens were prepared by extraction of small micro-fragments from the film. For this, the film surface was scratched with a thin diamond tip and the fragments were collected on holey carbon grids [33]. These fragments present edges with very small angles, so that, the TEM observation guarantees large transparent area useful for HRTEM images. The TEM images and SAED patterns were obtained using a Jeol TEM 200CX instrument, while for the HRTEM images was used a Topcon 002B electron microscope,

working at 200 kV. Cross-section TEM (XTEM) images were also obtained on sputtered samples.

The XPS measurements were performed in a complex Specs GmbH surface science setup that includes a photoemission chamber. The GeSiO samples were analyzed by using both an unmonochromatized Al K_α radiation (1486.61 eV) and a monochromatized Ag L_α radiation (2984.3 eV).

Electrical and photoconductivity investigations were performed on sol-gel samples, annealed by RTA, only. The setup used for these measurements contains a Janis CCS-450 cryostat (10 – 500 K), Keithley 6517A electrometer, Stanford SR 830 double lock-in amplifier, Newport monochromator, Newport light source 1000 W (Xe) (UV-VIS-NIR), LakeShore 331 temperature controller and Stanford SR 540 chopper. All measurements were performed on a computer-assisted set-up using a LabVIEW 8.5.1 development environment.

3. Results and Discussion TEM Investigations

The cross section TEM images showed that the GeSiO sol-gel layers are formed of amorphous nanodots with diameters in the range of 2 – 10 nm, uniformly distributed in an amorphous SiO_2 matrix, see Fig. 1 (Reprinted from Digest Journal of Nanomaterials and Biostructures **6** (1), 67-73 (2011), "Study of Ge nanoparticles embedded in an amorphous SiO_2 matrix with photoconductive properties", A. M. Lepadatu, I. Stavarache, T. F. Stoica, M. L. Ciurea, Figure 1, Copyright 2011, with permission from © INCDFM).
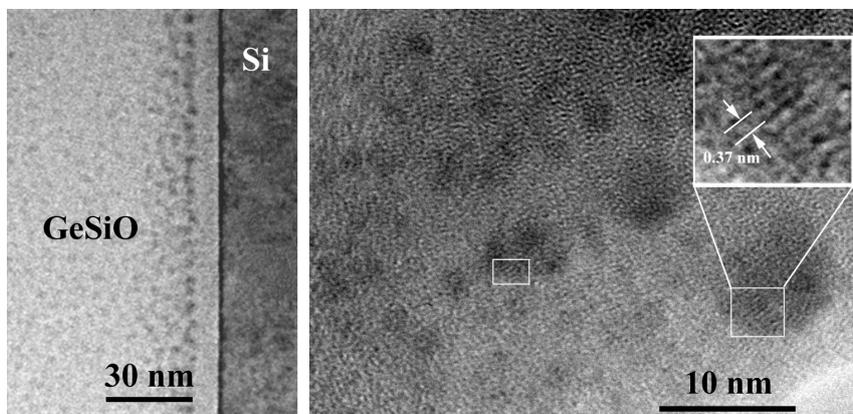

Fig. 1. XTEM image of a GeSiO (3 % Ge) sol-gel film annealed by RTA in N_2. Morphology of the interface with the Si substrate (left); some nanodots have small areas with lattice fringes like contrast, enlarged in the square frame (right) [15].

The interface between the nanodots and the SiO_2 matrix is not well defined, which is expected in the case of amorphous films. Thus, one can infer that the nanodots are Ge rich regions because the TEM contrast is dependent on the local

density and on the *Z* value of the atomic species. The density and size of nanodots are practically constant in the film thickness, except for the region near the interface with the silicon substrate (see Fig. 1 left). In this bottom region of the film, a SiO_2 band without nanodots, with a thickness of approximately 10 nm, is clearly visible. In its vicinity one finds Ge nanodots with larger sizes and density in comparison with the rest of the film.

One interesting feature is the presence of some nanodots which have small areas with lattice fringes like contrast (see Fig. 1 right). The periodicity of the lattice fringes is 0.36 ± 0.02 nm, that corresponds very well to the (111) lattice interfringe of tetragonal germanium phase. The most of the nanodots are amorphous, as the SAED pattern confirmed.

Another characteristic of the sol-gel films is the presence of coalescence starting-points (Fig. 2). No structural difference is observed between the samples annealed in N_2 and H_2. The main difference between various GeSiO sol-gel films is related to the variation of the nanodot density. The nanodot sizes slightly vary: for example if the Ge concentration grows from 3 % to 12 %, the average size of the nanodots increases from 3.8 to only 4.3 nm. The interfaces between all GeSiO sol-gel films and the Si substrate look similar. The SiO_2 clear band formed at the bottom of the film was attributed to the oxidation of the silicon substrate during the annealing process. In our opinion, this band is formed by nucleating of Ge rich nanodots that there are at the original interface and the increase of these nanodots by collecting of Ge species, so that no Ge diffusion takes place during the growing of SiO_2 band.
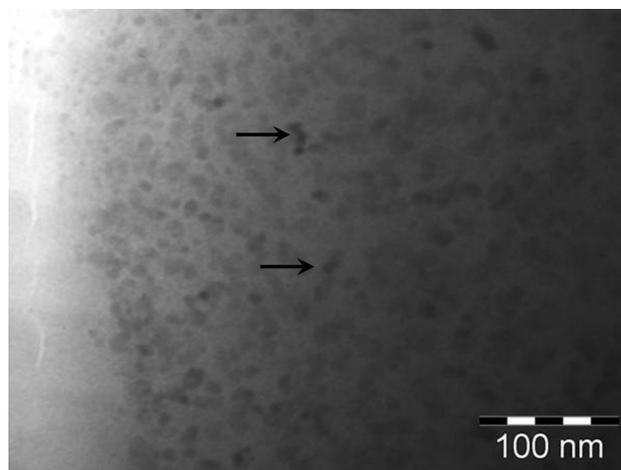

Fig. 2. Plan view TEM image of a sol-gel layer (12 % Ge) annealed in H_2. Some of the nanodots are connected (arrows).

In the case of the magnetron sputtered films, a more complex structure is evidenced. The concentration of Ge is of 40 %, a much larger value than that

obtained in the sol-gel layers. The morphology of these films is different of that of the sol-gel ones: thus, there are big Ge rich nanodots (20–50 nm) embedded in the amorphous SiO_2 matrix besides the smaller ones (5–15 nm) that are homogeneously distributed, as one can see in Fig. 3. The average size of 20 nm is evidenced. The low magnification XTEM image, presented in Fig. 3, shows the morphology of the layer in the middle of the GeSiO sputtered sample.
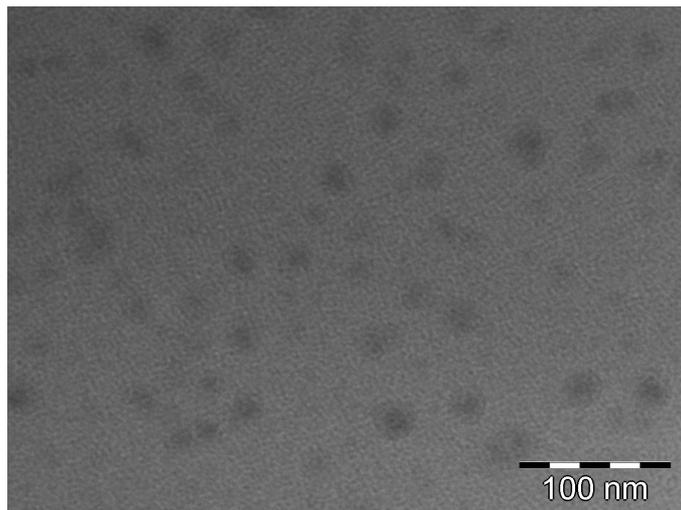

Fig. 3. Low magnification XTEM image in the middle of the
GeSiO (40 % Ge) sputtered sample.

The large nanodots show a well defined interface with the SiO_2 amorphous matrix. The local change of the TEM contrast in large nanodots at the slight tilting of specimen in the microscope gives a clear indication of the presence of a crystallized structure. This fact is confirmed by a SAED pattern, in Fig. 4 (Reprinted from Springer – Journal of Nanoparticle Research **13** (1), 221-232 (2011), "Structural investigations of Ge nanoparticles embedded in an amorphous SiO_2 matrix", I. Stavarache, A.-M. Lepadatu, N.G. Gheorghe, R.M. Costescu, G.E. Stan, D. Marcov, A. Slav, G. Iordache, T.F. Stoica, V. Iancu, V.S. Teodorescu, C.M. Teodorescu, and M.L. Ciurea, Figure 6, Copyright 2011, with kind permission from Springer Science+Business Media B.V.), where one can see that the main diffraction spots originate from the big nanocrystals, those with sizes larger than 40 nm.

The experimental data obtained from the SAED pattern measured on the GeSiO sputtered films were compared with the expected crystalline phases of germanium. The tetragonal phase of germanium was found to be the most suitable one for the sputtered films. It is already known from literature that this phase is metastable and appears under high pressure conditions only [34].
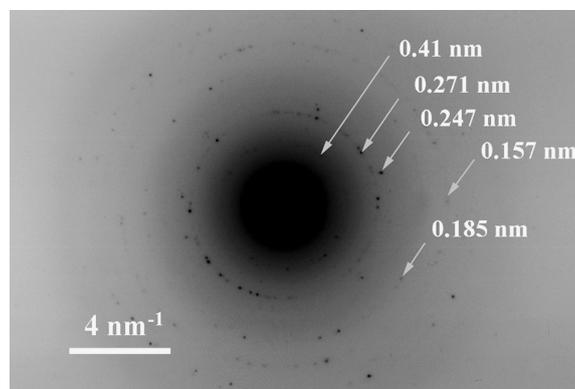
Fig. 4. SAED pattern of a sputtered film fragment: a number of clear
reflections could be measured in spite of the low contrast due to
the massive amorphous matrix [5].

The high resolution images of the sputtered GeSiO layers reveal two types of
Ge nanostructures (see Fig. 5, Reprinted from Springer – Journal of Nanoparticle
Research **13** (1), 221-232 (2011), "Structural investigations of Ge nanoparticles
embedded in an amorphous SiO_2 matrix", I. Stavarache, A.-M. Lepadatu, N.G.
Gheorghe, R.M. Costescu, G.E. Stan, D. Marcov, A. Slav, G. Iordache, T.F. Stoica,
V. Iancu, V.S. Teodorescu, C.M. Teodorescu, and M.L. Ciurea, Figure 7,
Copyright 2011, with kind permission from Springer Science+Business Media
B.V.). One consists of tetragonal Ge nanocrystals of approximately 10 nm diameter
(Fig. 5 left), with the lattice interfringe of about 0.45 nm [35]. The other forms a
network of Ge-rich nanostructures in the amorphous matrix (Fig. 5 right). In our
opinion, the high pressure tetragonal phase of Ge appears due to the stress field
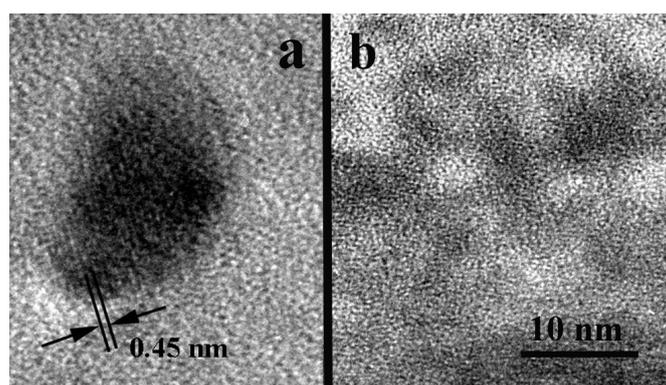developed in the GeSiO films during the annealing.

Fig. 5. HRTEM images on the sputtered specimen: a – crystallized nanodot
showing lattice fringes, b – a network of Ge-rich nanostructures
in the amorphous matrix [5].

We correlated the tetragonal phase of Ge with the stress field developed in the GeSiO layers due to contraction of the film structure during the annealing. Most likely, the preparation of TEM sample, namely the extraction of small micro-fragments from the film, permits us to put in evidence the tetragonal phase. In our opinion, the stress field could relax, during the preparation of TEM specimens by ion milling.

The wide-range survey XPS spectrum (shown in Fig. 6, Reprinted from Springer – Journal of Nanoparticle Research **13** (1), 221-232 (2011), "Structural investigations of Ge nanoparticles embedded in an amorphous SiO_2 matrix", I. Stavarache, A.-M. Lepadatu, N.G. Gheorghe, R.M. Costescu, G.E. Stan, D. Marcov, A. Slav, G. Iordache, T.F. Stoica, V. Iancu, V. S. Teodorescu, C.M. Teodorescu, and M.L. Ciurea, Figure 8, Copyright 2011, with kind permission from Springer Science+Business Media B.V.) measured for a magnetron sputtered GeSiO sample, using monochromatized Ag L_α, showed the presence of Ge, Si and O elements. One may observe traces of contaminants such as Zn or Na. The extracted binding energies were: 101,6 eV, 123,9 eV, 151,2 eV, 181,5 eV, and 1220,7 eV for the core levels Si 2p, Ge $3p_{3/2}$, Si 2s, Ge 3s, and Ge $3p_{3/2}$, respectively.
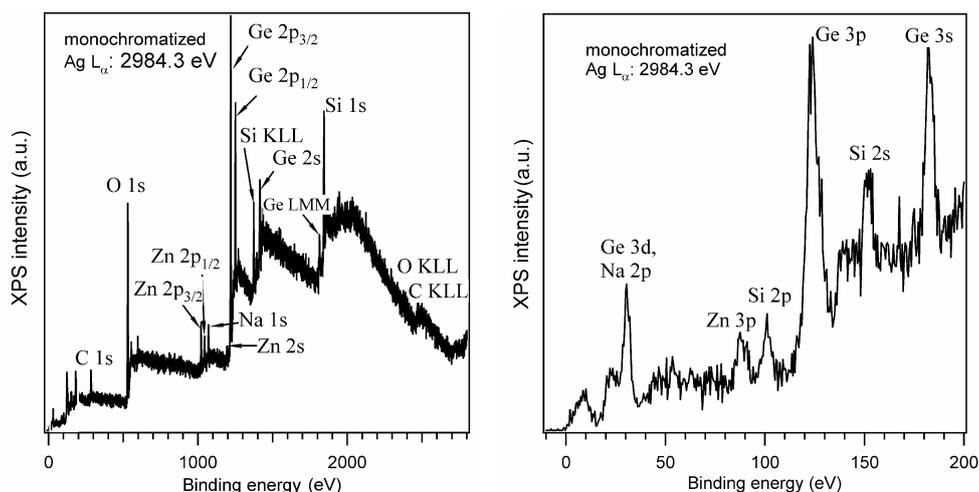

Fig. 6. a) Survey scan on a magnetron sputtered GeSiO layer, b) Detail of the survey scan in the region with binding energies lower than 200 eV. A monochromatized Ag L_α radiation was used [5].

In the case of sol-gel samples, a spectrum comprising the region of Si 2p-2s and Ge 3p-3s core levels was measured using unmonochromatized Al K_α radiation (see Fig. 7, Reprinted from Springer – Journal of Nanoparticle Research **13** (1), 221-232 (2011), "Structural investigations of Ge nanoparticles embedded in an amorphous SiO_2 matrix", I. Stavarache, A.-M. Lepadatu, N.G. Gheorghe,

R.M. Costescu, G.E. Stan, D. Marcov, A. Slav, G. Iordache, T.F. Stoica, V. Iancu, V.S. Teodorescu, C.M. Teodorescu, and M. L. Ciurea, Figure 9, Copyright 2011, with kind permission from Springer Science+Business Media B.V.). The extracted binding energies were: 104,2 eV, 126,2 eV, 155,2 eV, and 1221,3 eV for the core levels Si 2p, Ge $3p_{3/2}$, Si 2s, and Ge $3p_{3/2}$, respectively. This spectrum was compared with the ones corresponding to a clean Si (001) sample, to an oxidized germanium sample, and to a germanium sample after cleaning by ion sputtering.
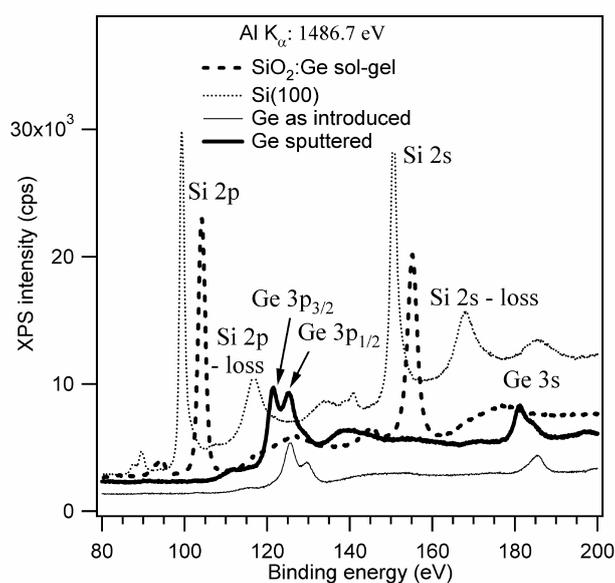

Fig. 7. Si 2p-2s and Ge 3p-3s core levels measured on a sol-gel prepared sample. This spectrum was compared with the ones corresponding to a clean Si (001) sample, to an oxidized germanium sample, and of a germanium sample after cleaning by ion sputtering [5].

The Ge $2p_{3/2}$ core level, shown in Fig. 8 (Reprinted from Springer – Journal of Nanoparticle Research **13** (1), 221-232 (2011), "Structural investigations of Ge nanoparticles embedded in an amorphous SiO_2 matrix", I. Stavarache, A.-M. Lepadatu, N.G. Gheorghe, R.M. Costescu, G.E. Stan, D. Marcov, A. Slav, G. Iordache, T.F. Stoica, V. Iancu, V.S. Teodorescu, C.M. Teodorescu, and M. L. Ciurea, Figure 10, Copyright 2011, with kind permission from Springer Science+Business Media B.V.), was measured on sol-gel and magnetron sputtered GeSiO films, and also on both an oxidized Ge crystal and a cleaned one by Ar^+ sputtering. The monochromatized Ag L_α radiation of 2984.3 eV was used. One can see that at the surface of the samples (the outermost 2 – 3 nm due to the finite photoelectron escape depth) only Ge in oxidised state can be found.
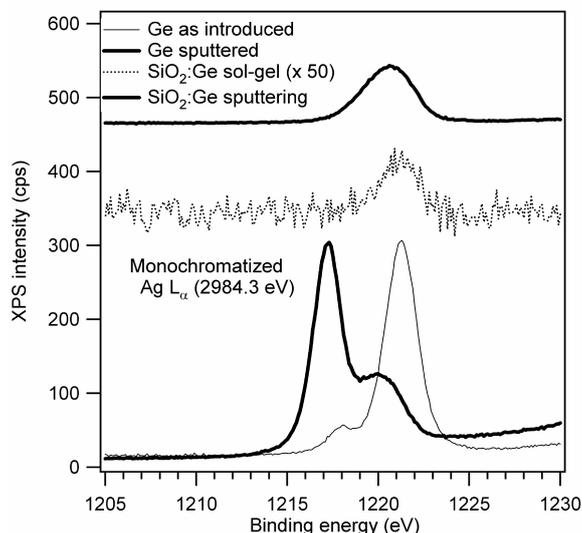
Fig. 8. Ge $2p_{3/2}$ core level measured, with monochromatized Ag L_α radiation, on sol-gel and magnetron sputtered GeSiO layers, and together with a Ge crystal as introduced and later cleaned by Ar^+ sputtering. The sol-gel spectrum is multiplied by 50, and the magnetron sputtered one is intentionally shifted upwards by + 450 cps [5].

The O 1s core level in oxidized Si (001) was compared with the corresponding spectrum in sol-gel GeSiO layer (see Fig. 9, Reprinted from Springer – Journal of Nanoparticle Research **13** (1), 221-232 (2011), "Structural investigations of Ge nanoparticles embedded in an amorphous SiO_2 matrix", I. Stavarache, A.-M. Lepadatu, N. G. Gheorghe, R. M. Costescu, G. E. Stan, D. Marcov, A. Slav, G. Iordache, T. F. Stoica, V. Iancu, V. S. Teodorescu, C. M. Teodorescu, and M. L. Ciurea, Figure 11, Copyright 2011, with kind permission from Springer Science+Business Media B.V.). One found a value of 533.7 eV for the binding energy of O 1s in GeSiO sample, and 532.3 eV for the oxidized silicon respectively. Comparing the experimental results with the ones from the NIST X-ray photoelectron spectroscopy database, one finds that silicon has a larger electronegativity in solid state than germanium.

The obtained values for core level binding energies are in good agreement with data reported in literature for clean Si and Ge samples. We found that the Si 2p core level binding energy of 101.6 eV, for magnetron sputtered samples fits well with the reported data for SiO [36] of 101.7 eV or for several SiO_x/Si structures [37]. Thus, in the magnetron sputtered GeSiO sample, silicon suboxides are formed. On the contrary, in the sol-gel sample, silicon oxide is formed.
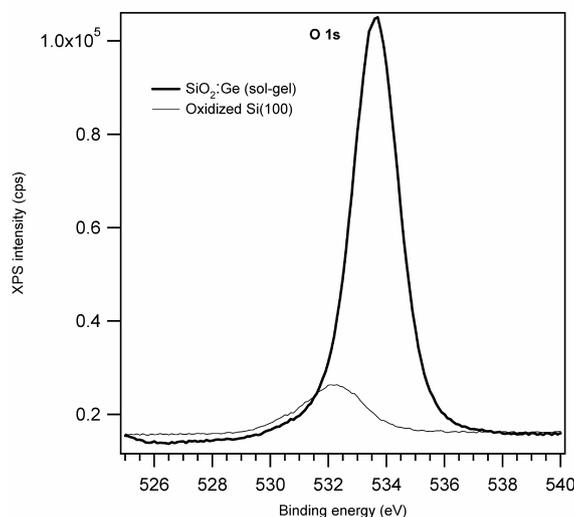
Fig. 9. O 1s core level in sol-gel film compared with the
one obtained on oxidized Si(001) [5].

In the sputtered sample, a lower binding energy (123.9 eV) for Ge is observed in comparison with the value corresponding to the oxidized Ge (125.6 eV) and to the data reported in literature for GeO_2, e.g. 125.3 eV [38]. This shows that at the surface of the magnetron sputtered samples germanium suboxides are also present. One can state that, the surface of the magnetron sputtered GeSiO films contains germanium and silicon suboxides, whereas the sol-gel one is composed of a mixture of GeO_2 and SiO_2. When one uses a target of amorphous SiO_2 covered with Ge pieces, it is typical to find suboxides at the surface of the deposited films. One can also see why the magnetron sputtered films are easier to be reduced than the sol-gel ones under equivalent conditions.

If one investigates in more detail the Si 2p, Ge $2p_{3/2}$ and $3p_{3/2}$ levels, by using the atomic sensitivity factors (ASF), as obtained empirically [39], will obtain 6 % of Ge/Si ratio at the sol-gel GeSiO (3 % Ge) sample surface, whereas at the magnetron sputtering sample surface the Ge concentration is three times higher than the Si one.

The $I - V$ characteristics, measured on sol-gel samples treated by RTA are presented in Fig. 10 (Reprinted from Digest Journal of Nanomaterials and Biostructures **6** (1), 67-73 (2011), "Study of Ge nanoparticles embedded in an amorphous SiO_2 matrix with photoconductive properties", A. M. Lepadatu, I. Stavarache, T. F. Stoica, M. L. Ciurea, Figure 2, Copyright 2011, with permission from © INCDFM). These curves were taken at RT, in the interval $0 - 1$ V, for both bias polarities. These samples, as already stated, are formed by amorphous Ge nanodots embedded in amorphous SiO_2 matrix. In these films are also present ordered Ge clusters close to Ge tetragonal phase that are produced during the RTA

treatment. A typical $I – V$ curve is asymmetric and has a weak rectifying behaviour, mainly given by the junction formed between the GeSiO film and Si substrate. This behaviour can be understood if we take into account that Ge nanodots, located at the interface SiO$_2$ clear band/GeSiO layer, can induce a depletion layer into the Si substrate. For a bias higher than 0.4 V, a linear dependence of the $I – V$ characteristic appears, so that this behaviour is dominated by the series resistance of the film.
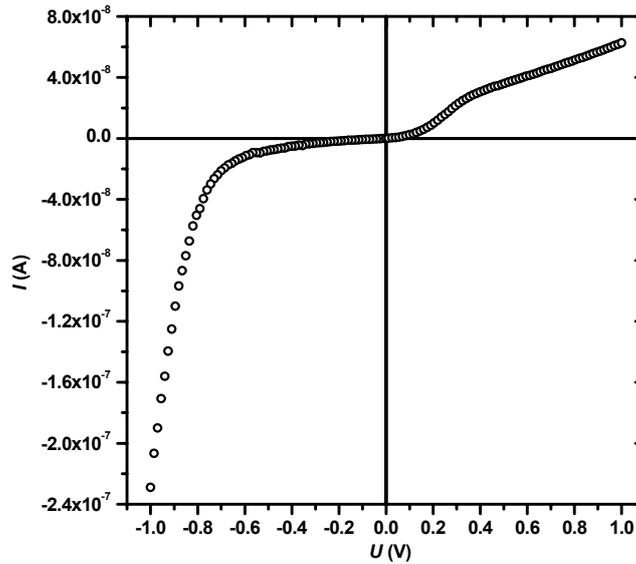

Fig. 10. Dark I – V curve taken at RT on a sol-gel sample treated by RTA [15].

The experimental curve was fitted (Fig. 11, Reprinted from Digest Journal of Nanomaterials and Biostructures **6** (1), 67-73 (2011)), "Study of Ge nanoparticles embedded in an amorphous SiO$_2$ matrix with photoconductive properties", A. M. Lepadatu, I. Stavarache, T. F. Stoica, M. L. Ciurea, Figure 3, Copyright 2011, with permission from © INCDFM) with the equation [40]:

$$I = I_S \exp\left(\frac{q(V - I \times R_S)}{nkT}\right)\left[1 - \exp\left(\frac{-q(V - I \times R_S)}{kT}\right)\right] \quad (1)$$

where I_S represents the reverse current at zero bias, q is the electron charge, n is the ideality factor, and R_S is a suitable series resistance. We found $I_S = 39$ pA, $n = 1.30$, and $R_S = 0.2$ MΩ.

On a reversed polarity, the process of thermionic emission is considered together with the electron-hole recombination in the depletion region that appears in the Si substrate, at the interface with the GeSiO film. For voltages higher than 0.4 V, the film contribution is dominant, thus the $I – V$ curve becomes linear.
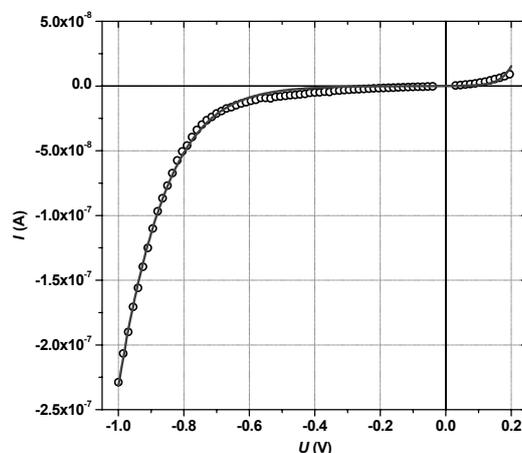
Fig. 11. The experimental dark I – V characteristic (open circles)
compared with the fit curve (continuous line) [15].

The temperature dependence of the conductance fits well the Mott law $\sigma \propto \exp\left[-\left(T_0/T\right)^{1/4}\right]$, which describes the transport mechanism of the VRH in amorphous materials. This is true only in the absence of dominant Coulomb interactions. A typical characteristic taken for a bias of 0.8 V is shown in Fig. 12. The curves measured for 0.5 and 0.9 V have a similar behaviour. The VRH transport in GeSiO sol-gel films can be explained by the hopping of electrons on localized states present in the amorphous film, including those associated with Ge clusters [11].

The photoconductive properties of the sol-gel films annealed under different conditions were investigated. The sol-gel films annealed by RTA show a very high photoconductivity, but those annealed in a heater under the same conditions (at the same temperature and atmosphere) are not photoconductive. Illuminating a sample annealed by RTA with white light from an incandescence lamp of 40 W, a big photocurrent appears. It is with 2 – 3 orders of magnitude bigger than the dark current. The spectral dependence of the photocurrent (I_f) was measured at RT in the 350–900 nm wavelength range. The curves were taken for different constant biases from 0 to 1 V, using modulated light, with an 80 Hz chopping frequency. The curves of the spectral dependence of the photocurrent, corresponding to both a not normalized to the incident light intensity and to a normalized ones are given in Fig. 13 a) and b) (Reprinted from Digest Journal of Nanomaterials and Biostructures **6** (1), 67-73 (2011), "Study of Ge nanoparticles embedded in an amorphous SiO_2 matrix with photoconductive properties", A.M. Lepadatu, I. Stavarache, T.F. Stoica, M.L. Ciurea, Figure 5, Copyright 2011, with permission from © INCDFM). One can see that the curves present a fine structure. The most important five maxima are located at 513, 724, 773, 804 and 862 nm.
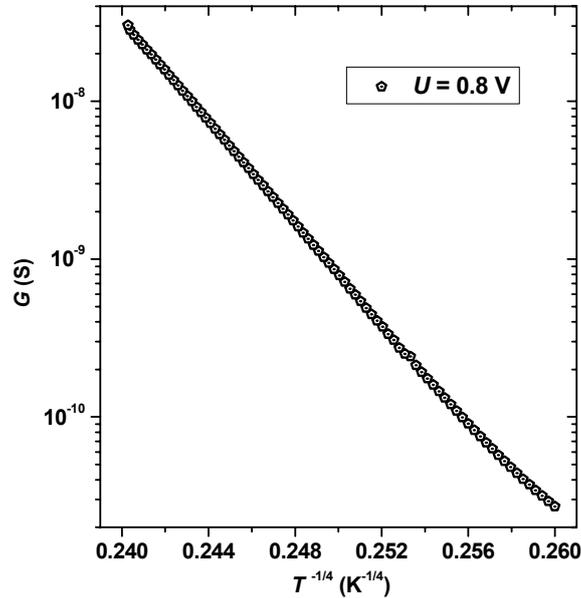
Fig. 12. Temperature dependence of the conductance
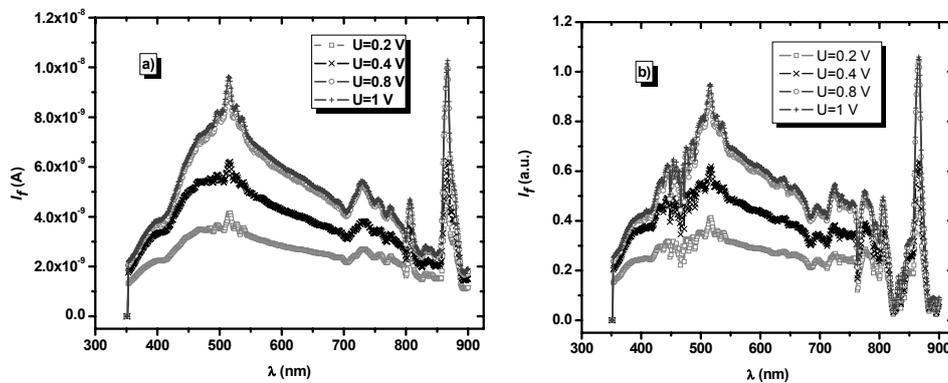taken for a bias of 0.8 V.

Fig. 13. Spectral dependence of the photocurrent measured at 0.2, 0.4, 0.8 and 1 V, corresponding to
both a) not normalized to the incident light intensity and b) to normalized ones, [15].

For the wavelengths corresponding to these maxima, photocurrent-voltage (I_f – V) characteristics were measured, using a continuous monochromatic light. The obtained curves are presented in Fig. 14 (Reprinted from Digest Journal of Nanomaterials and Biostructures **6** (1), 67-73 (2011), "Study of Ge nanoparticles embedded in an amorphous SiO_2 matrix with photoconductive properties", A.M. Lepadatu, I. Stavarache, T.F. Stoica, M.L. Ciurea, Figure 6, Copyright 2011,

with permission from © INCDFM) together with the dark $I - V$ one. These characteristics are not normalized to the incident light intensity. Looking at the curve measured under illumination with monochromatic light (862 nm), the photocurrent is with two orders of magnitude bigger than the dark current, if the sample is biased with 1 V.
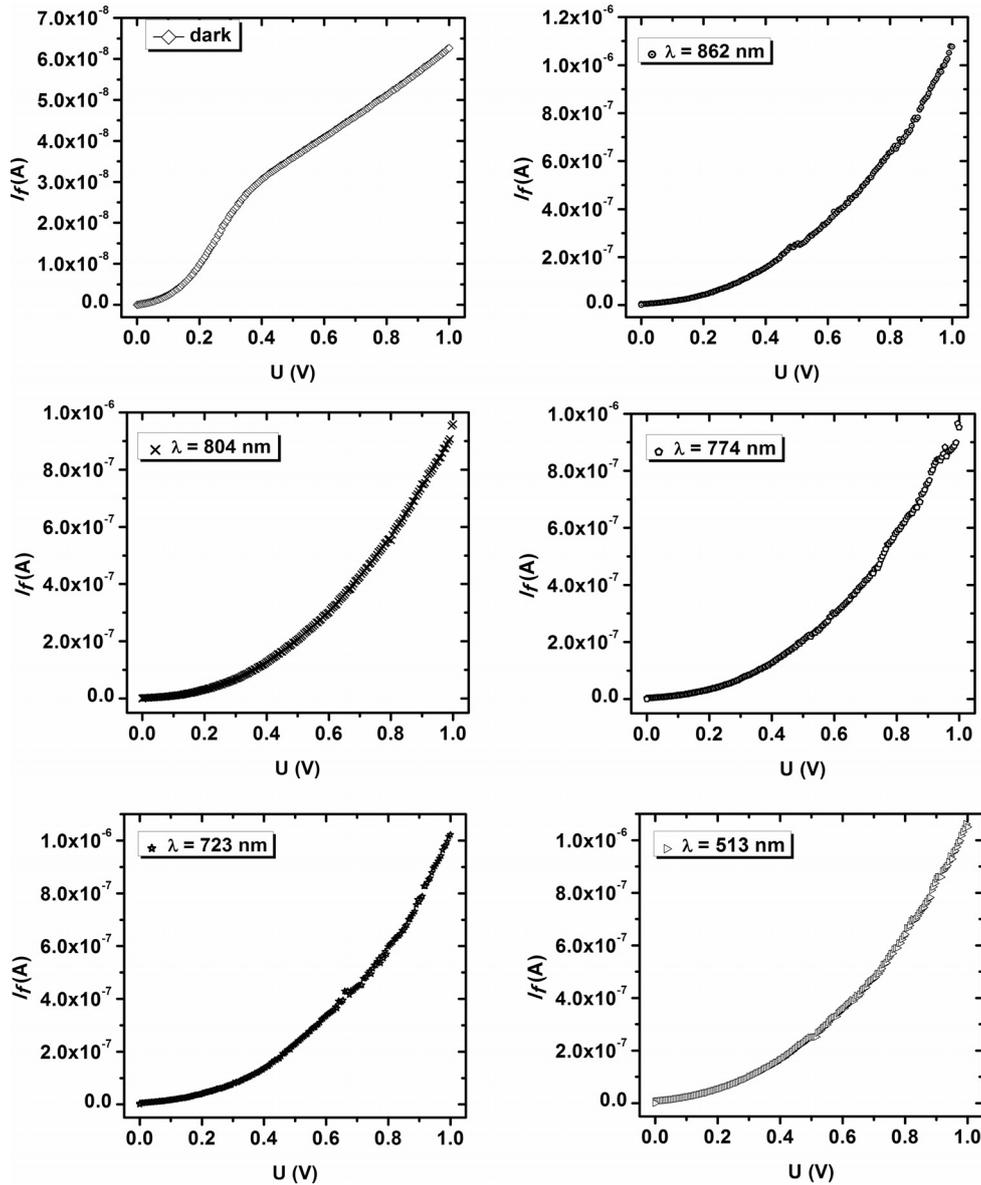

Fig. 14. $I_f - V$ characteristics for the wavelengths corresponding to the most important five maxima of the photocurrent in Fig. 13 b) and $I - V$ curve in dark [15].

The high photoconductivity can be explained by taking into account the Ge clusters and localized states (defects), produced during the RTA process, on which, the light absorption takes place [41]. The defects can also act as traps for a type of carriers (e.g electrons), thus increasing the lifetime of the other type (holes). The carriers with a longer lifetime will contribute in the photoconductivity. Also, different localized states/defects present in the film will produce the fine structure of the spectral curves.

4. Summary and Concluding Remarks

Films consisting of Ge nanodots embedded in amorphous SiO_2 matrix were prepared using two conventional deposition methods, sol-gel and magnetron-sputtering. Different investigations, namely structural investigations by TEM and XPS, electrical and photoconductivity measurements, were performed.

In the sol-gel films the major part of the Ge nanodots are amorphous. The average diameter gradually grows from 3.8 nm to 4.3 nm with the increase of Ge concentration from 3% Ge to 12% Ge. A 10 nm thick band of clear SiO_2 matrix, without nanodots, is present at the interface with the silicon substrate. This clear band was attributed to the oxidation of the silicon substrate during the annealing process. Near this band, one finds larger nanodots than in the rest of the film. In the sol-gel films, some of the nanodots present small areas with traces of (111) lattice interfringes corresponding to the tetragonal phase of germanium. No structural difference was observed between the samples annealed in N_2 and H_2.

In the case of sputtered GeSiO (40 % Ge) films two different Ge nanostructures were evidenced. One part of Ge forms big tetragonal nanocrystals, while the second part forms a network of Ge-rich amorphous nanostructures in the amorphous matrix. The magnetron sputtered layers consist of big Ge rich nanodots (20 – 50 nm) embedded in the amorphous SiO_2 matrix as well as smaller ones (5 – 15 nm) that are homogeneously distributed.

The tetragonal phase of germanium was found in the sputtered samples. This phase is metastable and appears under high pressure conditions only. The high pressure phase of Ge appears due to the stress field developed in the GeSiO layers during the annealing. Most likely, the preparation of TEM sample, namely the extraction of small micro-fragments from the film, permits us to put in evidence the tetragonal phase. Perhaps the stress field could relax, during the preparation of TEM specimens by ion milling.

The XPS measurements showed the presence of Ge, Si and O elements in the sol-gel and magnetron-sputtering films. At the surface of sol-gel films one finds a mixture of GeO_2 and SiO_2, whereas the sputtered ones contain germanium and silicon suboxides. The surface of GeSiO samples consist of a greater Ge concentration than the one present in the volume of the films.

The $I - V$ characteristics, measured on sol-gel samples treated by RTA, are asymmetric and have a weak rectifying behaviour, mainly given by the junction formed between GeSiO film and Si substrate. The transport mechanism of the variable range hopping in amorphous materials was evidenced. This can be explained by the hopping of electrons on localized states present in the amorphous film, including those associated with Ge clusters.

The GeSiO sol-gel films annealed by RTA show a very high photoconductivity. The curves of spectral dependence of the photocurrent present a fine structure with five main maxima. The high photoconductivity can be explained by taking into account the Ge clusters and localized states (defects) produced during the RTA process, on which, the light absorption takes place.

References

[1]   NOGAMI M. and ABE Y., Appl. Phys. Lett. **65**, p. 2545, 1994.
[2]   ZHANG B., SHRESTHA S., GREEN M.A., and CONIBEER G., Appl. Phys. Lett. **96**, p. 261901, 2010.
[3]   YANG H., YAO Xi, WANG X., XIE S., FANG Y., LIU S., and GU X., J. Phys. Chem. B **107**, p. 13319, 2003.
[4]   KOLOBOV A.V., WEI S.Q., YAN W.S., OYANAGI H., MAEDA Y., and TANAKA K., Phys Rev. B **67**, p. 195314, 2003.
[5]   STAVARACHE I., LEPADATU A.-M., GHEORGHE N.G., COSTESCU R.M., STAN G.E., MARCOV D., SLAV A., IORDACHE G., STOICA T.F., IANCU V., TEODORESCU V.S., TEODORESCU C. M., AND CIUREA M.L., J. Nanopart. Res. **13**, p. 221, 2011.
[6]   KNEBEL S., KYRIAKIDOU A., BRACHT H., RÖSNER H., and WILDE G., Appl. Phys. A: Mater. Sci. Process, DOI 10.1007/s00339-010-6156-4.
[7]   RAY S.K. and DAS K., *Opt. Mater.* **27**, p. 948, 2005.
[8]   COSENTINO S., MIRABELLA S., MIRITELLO M., NICOTRA G., LO SAVIO R., SIMONE F., SPINELLA C., and TERRASI A., Nanoscale Res. Lett. **6**, p. 135, 2011.
[9]   GACEM K., El HDIY A., TROYON M., BERBEZIER I., SZKUTNIK P.D., KARMOUS A., and RONDA.A., J. Appl. Phys. **102**, p. 093704, 2007.
[10]   El HDIY A., Gacem K., Troyan M., Ronda A., Bassani F., and Berzebier I., J. Appl. Phys. **104**, p. 063716, 2008.
[11]   FUJII M., INOUE Y., HAYASHI S., and YAMAMOTO K., Appl. Phys. Lett. **68**, p. 3749, 1996.
[12]   FUJII M., MAMEZAKI O., HAYASHI S., and YAMAMOTO K., J. Appl. Phys. **83**, p. 1507, 1998.
[13]   ZHANG B., YAO Y., PATTERSON R., SHRESTHA S., GREEN M.A., and CONIBEER G., Nanotechnology **22**, p. 125204, 2011.
[14]   CASTRUCCI P., GOBBO Del S., SPEISER E., SCARSELLI M., De CRESCENZI M., AMIARD G., RONDA A., and BERBEZIER I., J. Non-Cryst. Solids **356**, p. 1940, 2010.
[15]   LEPADATU A.M., STAVARACHE I., STOICA T.F., ANDand CIUREA M.L., Digest J. Nanomater. Bios. **6**, p. 67, 2011.

[16]   STOICA T.F., GARTNER M., TEODORESCU V.S., and STOICA T., J. Optoelectron. Adv. Mater. **9**, p. 3271, 2007.
[17]   KANJILAL A., LUNDSGAARD HANSEN J., GAIDUK P., NYLANDSTED LARSEN A., CHERKASHIN N., CLAVERIE A., NORMAND P., KAPELANAKIS E., SKARLATOS D., and TSOUKALAS D., Appl. Phys. Lett. **82**, p. 1212, 2003.
[18]   ZHANG L., YE H., HUANGFU Y.R., ZHANG C., and LIU X., Appl. Surf. Sci. **256**, p. 768, 2009.
[19]   SHEN J.K., WU X.L., TAN C., YUAN R.K., and BAO X.M., Phys. Lett. A **300**, p. 307, 2002.
[20]   PEIBST R., SOUSA de J.S., and HOFMANN K.R., Phys. Rev. B **82**, p. 195415, 2010.
[21]   SRINIVASA RAO N., PATHAK A.P., SATHISH N., DEVARAJU G., SAIKIRAN V., KULRIYA P.K., AGARWAL D.C., SAI SARAVANAN G., AVASTHI D.K., Solid State Commun. **150**, p. 2122, 2010.
[22]   FUKUDA H., SAKUMA S., YAMADA T., NOMURA S., NISHINO M., HIGUCHI T., and OHSHIMA S., J. Appl. Phys. **90**, p. 3524, 2001.
[23]   CHEN Q., LU T., XU M., MENG C., HU Y., SUN K., and SHLIMAK I., Appl Phys Lett **98**, p. 073103, 2011.
[24]   SRINIVASA RAO N., PATHAK A.P., DEVARAJU G., SAIKIRAN V., Vacuum **85**, p. 927, 2011.
[25]   DAS S., SINGHA R.K., GANGOPADHYAY S., DHAR A., and RAY S.K., J. Appl. Phys. **108**, p. 053510, 2010.
[26]   DAS S., SINGHA R.K., MANNA S., GANGOPADHYAY S., DHAR A., and RAY S.K., *J. Nanopart. Res.* **13**, p. 587, 2011.
[27]   BULJAN M., PINTO S.R.C., ROLO A.G., . MARTÍN-SÁNCHEZ J, GOMES M.J.M., GRENZER J., MÜCKLICH A., BERNSTORFF S., AND HOLÝ V., Phys. Rev. B **82**, p. 235407, 2010.
[28]   CHATTERJEE S., J. Phys.: D Appl. Phys. **41**, p. 055301, 2008.
[29]   AKTAĞ A., YILMAZ E., MOGADDA N.A.P., AYGUN G., CANTAS A., TURAN R., Nucl. Instr. *Meth.* Phys. Res **B 268**, p. 3417, 2010.
[30]   TZENG S.S. and LI P.W., Nanotechnology **19**, p. 235203, 2008.
[31]   HONG S.H., KIM M.C., JEONG P.S., CHOI S.-H., and KIM K.J., Nanotechnology **19**, p. 305203, 2008.
[32]   STAVARACHE I., LEPADATU A.-M., TEODORESCU V., STOICA T., PASUK I., STAN G., IANCU V., AND CIUREA M.L., CAS 2010 Proceedings IEEE CN CFP10CAS-PRT; 33nd International Semiconductor Conference (CAS 2010, Sinaia, 11–13 October), **1**, p. 77, 2010.
[33]   TEODORESCU V.S. and BLANCHIN M.G., Microscopy and Microanalysis **15**, p. 15, 2009.
[34]   WOSYLUS A., PROTS Y., SCHNELLE W., HANFLAND M., and SCHWARZ U., Zeitschrift für Naturforschung B **63b**, p. 608, 2008.
[35]   Powder Diffraction File, PDF No: 18-0549. Available via http://www.icdd.com.
[36]   NGUYEN T.P. and LEFRANT S., J. Phys. Cond. Matter. **1**, p. 5197, 1989.
[37]   KERKHOF F.P.J., MOULIJN J.A., and HEERES A., J. Electron. Spectrosc. Relat. Phenom. **14**, p. 453, 1978.
[38]   MORGAN W.E. and WAZER Van J.R., J. Phys. Chem. **77**, p. 964, 1973.
[39]   WAGNER C.D., DAVIS L.E., ZELLER M.V., TAYLOR J.A., RAYMOND R.M., and GALE L.H., Surf. Interf. Anal. **3**, p. 211, 1981.
[40]   RAY A.K., MABROOK M.F., NABOK A.V., and BROWN S., J. Appl. Phys. **84**, p. 3232, 1998.
[41]   YANG H., YAO X., XIE S., WANG X., LIU S., FANG Y., GU X., and WANG F., Opt. Mater. **27**, p. 725, 2005.